Adsorption of Group-IV Elements on Graphene, Silicene, Germanene, Stanene: Dumbbell Formation

ARTICLE *in* THE JOURNAL OF PHYSICAL CHEMISTRY C · DECEMBER 2014

Impact Factor: 4.77 · DOI: 10.1021/jp5106554 · Source: arXiv

4 AUTHORS:

Ongun Ozcelik
Princeton University
27 PUBLICATIONS **224** CITATIONS
SEE PROFILE

Deniz Keçik
Bilkent University
8 PUBLICATIONS **27** CITATIONS
SEE PROFILE

Engin Durgun
Bilkent University
71 PUBLICATIONS **1,654** CITATIONS
SEE PROFILE

Salim Ciraci
Bilkent University
307 PUBLICATIONS **11,646** CITATIONS
SEE PROFILE

THE JOURNAL OF PHYSICAL CHEMISTRY C

Article

pubs.acs.org/JPCC

Adsorption of Group IV Elements on Graphene, Silicene, Germanene, and Stanene: Dumbbell Formation

V. Ongun Özçelik,[†,‡] D. Kecik,[†,‡] E. Durgun,*[,†,‡] and S. Ciraci*[,§]

[†]UNAM-National Nanotechnology Research Center, [‡]Institute of Materials Science and Nanotechnology, and [§]Department of Physics, Bilkent University, 06800 Ankara, Turkey

ABSTRACT: Silicene and germanene derivatives constructed from periodic dumbbell units play a crucial role in multilayers of these honeycomb structures. Using first-principles calculations based on density functional theory, here we investigate the dumbbell formation mechanisms and energetics of Group IV atoms adsorbed on graphene, silicene, germanene, and stanene monolayer honeycomb structures. The stabilities of the binding structures are further confirmed by performing *ab initio* molecular dynamics calculations at elevated temperatures, except for stanene which is subject to structural instability upon the adsorption of adatoms. Depending on the row number of the adatoms and substrates we find three types of binding structures, which lead to significant changes in the electronic, magnetic, and optical properties of substrates. In particular, Si, Ge, and Sn adatoms adsorbed on silicene and germanene form dumbbell structures. Furthermore, dumbbell structures occur not only on single-layer, monatomic honeycomb structures but also on their compounds like SiC and SiGe. We show that the energy barrier to the migration of a dumbbell structure is low due to the concerted action of atoms. This renders dumbbells rather mobile on substrates to construct new single and multilayer Si and Ge phases.

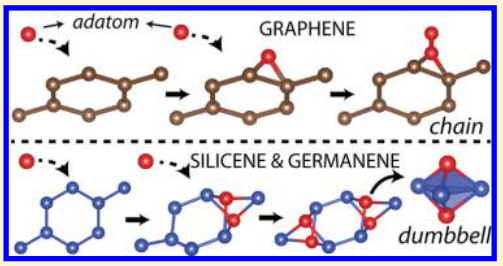

INTRODUCTION

Recent theoretical and experimental studies have proven that silicon,[1−5] germanium,[6−9] compound semiconductors,[6] α-silica,[10] α-tin,[11−14] transition metal oxides, and dichalcogenides[15−18] can have stable, single-layer honeycomb structures like graphene. However, in contrast to suspended graphene which can be easily exfoliated from 3D layered graphite, free-standing single layers of Si, Ge, and Sn were not synthesized yet since these elements do not exist as 3D layered bulk phases in nature. Therefore, it is a very accessible way (and the only possible way so far) to synthesize single layers of Si (i.e., silicene), Ge (i.e., germanene), and Sn (i.e., stanene) on suitable substrates like silver and gold. Under these circumstances, the growth of stable multilayers of silicene was recently achieved.[7,19,20] After the synthesis of thick layered silicene, the possibility of the layered bulk allotrope of silicon has been explored, and stable bulk phases of Si have been predicted, which show a layered character and display electronic and optical properties different from those of the well-known cubic diamond structure.[21] These results were further supported by the experimental data collected from multilayer silicene grown on Ag(111) substrates.[7,19,20]

Understanding the structure of layered silicene is of particular importance in a wide range of applications from electronics design to Li-ion storage for batteries.[22] Scanning tunneling microscopy (STM) measurements aiming at the understanding of the structure of multilayer silicene grown on a Ag(111) substrate[7,19] revealed that silicene layers have a ($\sqrt{3}\times\sqrt{3}$) supercell with honeycomb structure. Earlier, theoretical studies found that the adsorption of a Si adatom on silicene is exothermic and results in a dumbbell (DB) structure, where the Si adatom attached to the top side on silicene pushes the host Si atom down to form a cage.[23−26] Recently, silicene derivatives constructed from periodic patterns of DB structures were found to be energetically more favorable.[27] Additionally, stacking of these DB-based silicene derivatives reproduced the structure data obtained from STM measurements of grown multilayers. These findings have pointed out that the grown multilayer silicenes may, in fact, be constructed from the dumbbell-based single-layer phases of silicene.[27] Furthermore, our recent letter[8] shows that stable DB structures can occur not only on silicene but also on germanene. Then the important question that remains to be answered is whether DB-based single-layer phases can be common to all Group IV elements.

Motivated by the remarkable aspects of the DB structures, their insight on the layered allotropes, and coverage-dependent phases revealed,[8] in this study we carried out an extensive analysis of the adsorption of the Group IV adatoms (C, Si, Ge, and Sn) on the single-layer honeycomb substrates constructed from these atoms (i.e., graphene, silicene, germanene, and stanene) amounting to 16 possible adatom + substrate combinations. Furthermore, we extended our analysis to include single-layer compounds, such as SiC and SiGe. The question of whether the DB structure is common to all of these systems has been our starting point. Important findings of our study can be summarized as: (i) Three different types of equilibrium binding structures can occur when Group IV adatoms adsorb on graphene, silicene, and germanene. These

Received: October 23, 2014
Revised: December 4, 2014
Published: December 9, 2014

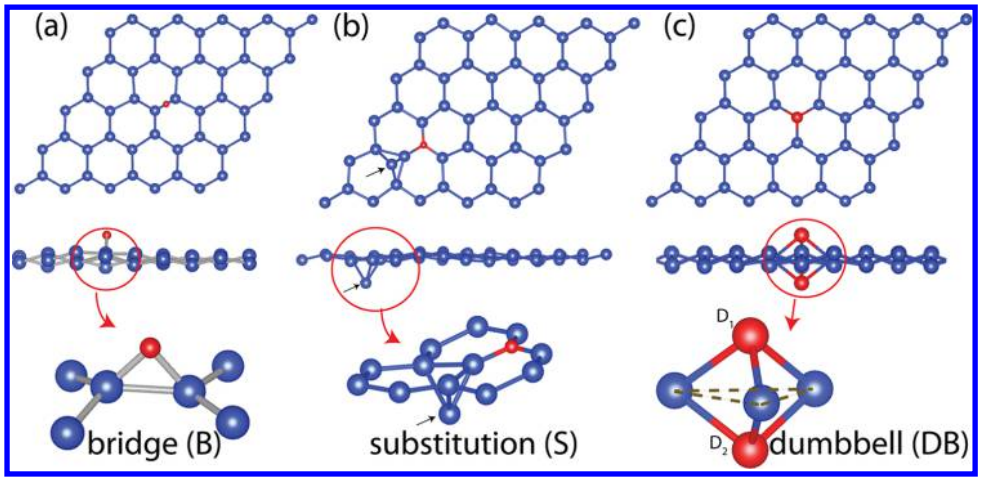

Figure 1. Side and top views of various types of equilibrium atomic structures, which occur when a Group IV element (C, Si, Ge, and Sn) is adsorbed on the single-layer honeycomb structure constructed from Group IV elements (graphene, silicene, and germanene). (a) A Group IV adatom adsorbed at the bridge site, i.e., B-site. (b) Substitution of silicene or germanene host atoms by the carbon adatom, i.e., S-site. The small arrows indicate the host Si atom that is pushed down after the substitution of the C adatom. (c) Dumbbell (DB) structure constructed by Si, Ge, and Sn adatoms adsorbed on silicene and germanene. D_1 and D_2 are dumbbell atoms; D_1 is the adatom, and D_2 is the host atom pushed down by D_1. Adatom and single-layer substrate atoms are described by red and blue balls, respectively.

Table 1. Adsorption of Group IV Adatoms on Single-Layer Honeycomb Structures of Group IV Elements, Namely, Graphene, Silicene, and Germanene in a 5 × 5 Supercell[a]

substrate	adatom	structure	d (Å)	a (Å)	μ (μ_B)	elec. state (eV)	E_b (eV)
graphene	C	B	1.52	12.35	0.4	metal	1.670
graphene	Si	B	2.21	12.39	1.6	metal	0.799
graphene	Ge	B	2.41	12.41	1.6	metal	0.711
graphene	Sn	B	2.69	12.36	1.6	metal	0.808
silicene	C	S	1.96	19.24	2.0	0.26 (0.66)	5.890
silicene	Si	DB	2.40 (2.70)	19.28	2.0	0.08 (0.50)	4.017
silicene	Ge	DB	2.51 (2.80)	19.31	2.0	0.06 (0.47)	3.612
silicene	Sn	DB	2.73 (2.97)	19.21	2.0	0.09 (0.38)	3.200
germanene	C	S	2.02	20.07	2.0	0.10 (0.42)	5.026
germanene	Si	DB	2.46 (2.83)	19.87	2.0	0.06 (0.39)	3.200
germanene	Ge	DB	2.57 (2.93)	19.89	2.0	0.06 (0.35)	3.397
germanene	Sn	DB	2.76 (3.09)	20.01	2.0	0.08 (0.30)	3.080

[a]Substrate (graphene, silicene, or germanene); adatom; types of binding structure (B = bridge; S = substitution; DB = dumbbell); nearest adatom−substrate atom distance d (values in parentheses are D_1−D_2 distance in DB structures); the lattice constant of the hexagonal unit cell of adatoms, a; magnetic moment per supercell (μ); electronic state (numeral indicates the minimum band gap in eV, HSE band gaps are given in parentheses); binding energy, E_b.

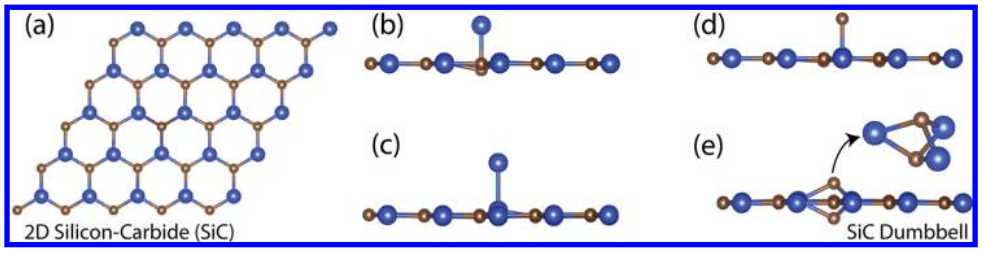

Figure 2. Equilibrium binding structures of C and Si adatoms on the graphene-like structure of SiC. (a) Top view of compound SiC displaying a planar honeycomb structure. (b) Si adatom on the C host atom. (c) Si adatom on the Si host atom. (d) C adatom on the Si host atom is adsorbed at the head-on positions rather than forming a dumbbell structure. (e) C adatom on the host C atom of SiC forming a DB structure. Si and C atoms are indicated by large blue and small brown balls, respectively.

are specified as bridge bonding (B), substitutional (S), and dumbbell (DB). (ii) DB structure is not observed if the adatom or monatomic, single-layer honeycomb substrate involves carbon atoms. (iii) A structural instability is induced when one atom from Group IV elements is adsorbed on stanene, whereby the honeycomb structure is disrupted even at T = 0 K. (iv) In silicene and germanene, the C adatom substitutes host Si and Ge atoms. (v) Si, Ge, and Sn form stable DB structures on silicene, as well as germanene, with critical electronic, magnetic, and optical properties. (vi) In compound single-layer honeycomb structure of silicon carbide, the C adatom forms a dumbbell structure, similar to Si and Ge adatoms adsorbed on a

dx.doi.org/10.1021/jp5106554 | J. Phys. Chem. C 2015, 119, 845−853

single-layer SiGe compound. (vii) We showed that the energy barrier for the migration of DBs is not high due to the concerted process of atoms at close proximity. This situation renders DB structures of Si, Ge, and Sn mobile on silicene and germanene and paves the way to grow new single-layer phases having different periodic patterns of the DBs. These phases, in turn, can offer alternatives to grow thin films or layered bulk structures and their compounds with diverse properties. (viii) The present results indicate that novel electronic, magnetic, and optical properties can be achieved through the periodic coverage of graphene, silicene, and germanene by Group IV adatoms.

METHOD

Our predictions were obtained from first-principles pseudopotential calculations based on the spin-polarized density functional theory (DFT)[28,29] within the generalized gradient approximation (GGA) including van der Waals corrections.[30] Projector-augmented wave potentials (PAWs)[31] were used, and the exchange-correlation potential was approximated with the Perdew–Burke–Ernzerhof (PBE) functional.[32] The adsorption of a single adatom on various single-layer honeycomb structures was simulated by using the periodically repeating supercell method in terms of 5 × 5 supercells comprising 50 host atoms and 1 adatom. The Brillouin zone (BZ) was sampled according to the Monkhorst–Pack scheme, where the convergence in energy as a function of the number of k-points was tested. The k-point sampling of (21 × 21 × 1) was found to be suitable for the BZ corresponding to the primitive unit cells of substrates. For larger supercells this sampling has been scaled accordingly. For the case of the 5 × 5 cell used in this study, the k-point sampling was chosen as 5 × 5 × 1. Atomic positions were optimized using the conjugate gradient method, where the total energy and atomic forces were minimized. The energy convergence value between two consecutive steps was chosen as 10^{-5} eV. A maximum force of 0.002 eV/Å was allowed on each atom. Numerical calculations were carried out using the VASP software.[33] Since the band gaps are underestimated by standard DFT methods, we also carried out calculations using the Heyd–Scuseria–Ernzerhof (HSE) hybrid functional,[34,35] which is constructed by mixing 25% of the Fock exchange with 75% of the PBE exchange and 100% of the PBE correlation energy. For the optical properties computed at the random phase approximation (RPA) level,[36] a (127 × 127 × 1) k-point grid and a total of 96 bands were undertaken for a proper description of the dielectric function.

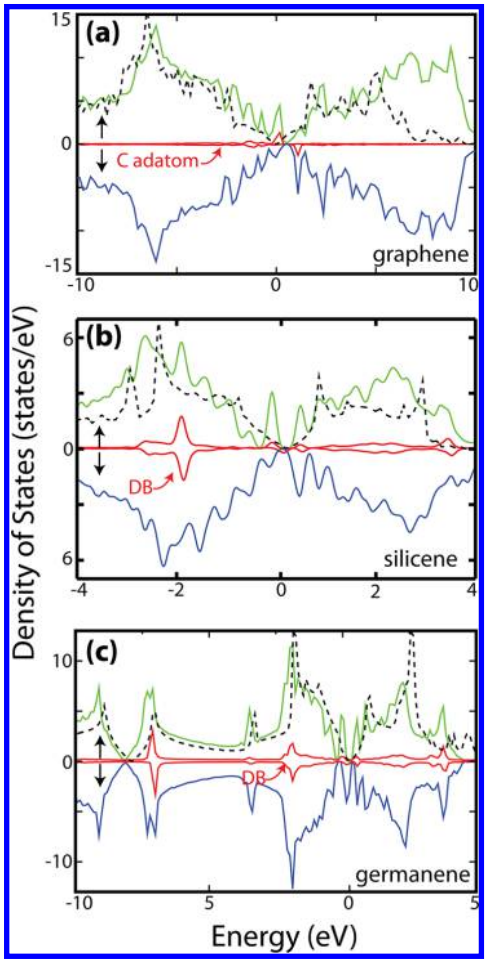

Figure 3. Total density of states for (a) C on graphene, (b) Si on silicene, and (c) Ge on germanene. The partial DOS of the adatoms are indicated by red lines and multiplied by a factor of 2 for better visualization. Spin up and spin down states are shown with green and blue lines, respectively. DOS of pure graphene, silicene, and germanene are also indicated by the dashed curves in the plots.

The binding energy, E_b, was calculated using the expression $E_b = E_T[A] + E_T[\text{sub}] - E_T[A + \text{sub}]$ in terms of the optimized total energies of the adatom $E_T[A]$, of the bare substrate (graphene, silicene, etc.) $E_T[\text{sub}]$, and of the adatom adsorbed on the substrate $E_T[A + \text{sub}]$, all calculated in the same supercell. Positive values of E_b indicate that the adsorption of the adatom is an exothermic process and is energetically favorable.

Further to the conjugate gradient method, the stabilities of structures were tested by *ab initio* molecular dynamic (MD) calculations performed at finite temperatures. A Verlet algorithm was used to integrate Newton's equations of motion with time steps of 2 fs. We carried out MD calculations at temperatures T = 200 K, T = 400 K, T = 600 K, T = 800 K, and T = 1500 K, each lasting 1 ps and totaling 5 ps for each adatom + substrate system. To maintain the system in the desired constant temperature, the velocities of atoms were rescaled in each time step allowing a continuous increase or decrease of the kinetic energy.

Equilibrium Structures and Energetics. Adsorption of Group IV atoms on single-layer graphene, silicene, germanene, and stanene is studied in terms of the periodically repeating supercell method, where one adatom is adsorbed in each 5 × 5 supercell. Since the adatom–adatom coupling between the 5 × 5 supercells is minute, this system can be taken to mimic the single, isolated adatom and the local reconstruction thereof. The equilibrium binding structures and corresponding local reconstruction of C, Si, Ge, and Sn adatoms on graphene, silicene, germanene, and stanene substrates have been explored by placing the adatoms at various sites and optimizing the atomic structures using the conjugate gradient method. The optimized binding structures, namely, B, S, and DB, are schematically described in Figure 1. The corresponding structural parameters, binding energy, and magnetic and electronic structure are summarized in Table 1. All of the Group IV adatoms on stanene give rise to massive local reconstruction leading to the destruction of honeycomb structure in the 5 × 5 supercell. This structural instability occurring even in the course of structure optimization using the

dx.doi.org/10.1021/jp5106554 | J. Phys. Chem. C 2015, 119, 845–853

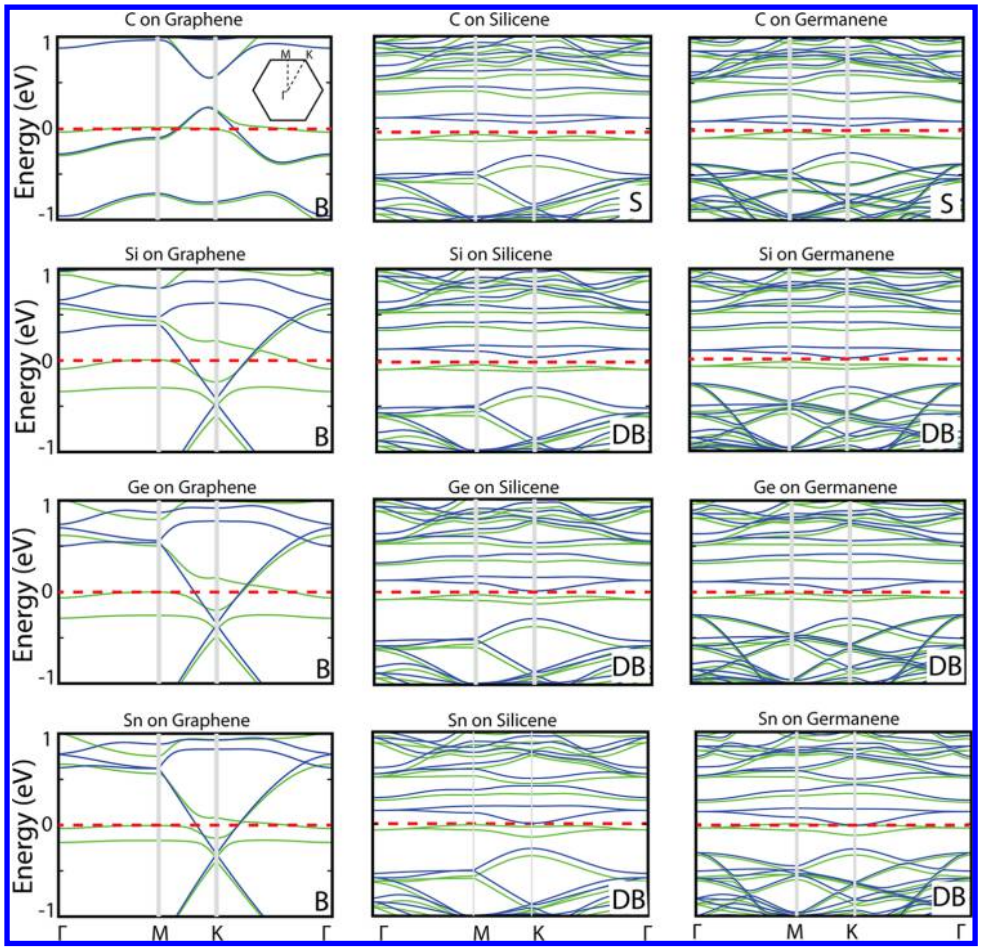

Figure 4. Electronic band structures of monolayer graphene, germanene, and silicene with adatoms C, Si, Ge, and Sn, which form a 5 × 5 supercell or pattern. In the spin-polarized systems, spin up and spin down bands are shown with green and blue lines. The zero of energy shown by a red dashed line is set to the energy of the highest occupied state. Binding structures (as B, S, DB) are indicated in each panel. Brillouin zone and symmetry directions are shown by inset.

conjugate gradient method at T = 0 K is critical since it does not comprise artificial effects, like small unit cells enhancing stability, etc. The instability followed by adatom adsorption implies that the single-layer honeycomb structure of Sn is in a shallow minimum and is prone to structural deformations.

In particular, the carbon atom having electronic structure $1s^2 2s^2 2p^6$ behaves rather differently from the rest of the Group IV elements. For example, owing to the relatively smaller C−C bond the $\pi-\pi$ interaction stabilizes the planar structure of graphene attained by sp^2 bonding, whereas single-layer honeycomb structures of silicene, germanene, and stanene are stabilized through buckling of atoms ensuring sp^3-like hybridization to compensate the weakening of $\pi-\pi$ interaction. For the same reason, while carbon atoms can make stable monatomic chain structure (cumulene and polyyne),[37−40] suspended monatomic chain structure cannot be stable for the rest of the Group IV elements.

Carbon adatom binds to graphene at the B-site with a binding energy of $E_b \simeq 1.7$ eV as shown in Figure 1(a). Even if the C adatom is placed at the top site (which is 0.86 eV less favorable), it prefers to migrate back to the B-site.[40,41] As the C adatom coverage increases from 9 × 9 to 2 × 2, the binding energy can vary, but the B-site continues to be the most favorable adsorption site. The binding energy was calculated to be 2.3 eV within the local density approximation, which is known to yield over binding.[40,41] Upon the adsorption of the C adatom at the B-site, while the underlying C−C bond of graphene elongates and causes the weakening of sp^2 bonding, new bonds are formed between 2p orbitals of the C adatom and graphene π-orbitals. The orbital composition and charge density of these new bonds were presented, and the long-range interaction between C adatoms was revealed.[40,41] A chain structure situated perpendicular to the graphene can nucleate if additional C adatoms are placed at close proximity to the C adatom at the B-site. On the other hand, the carbon adatom adsorbed on silicene and germanene replaces the host Si or Ge atoms, respectively. These host atoms, which are removed from their position at the corner of the hexagon, slightly dip below and move toward the center of the hexagon. They form three back bonds with the three nearest atoms at the corners of the hexagon as shown in Figure 1(b). Substitutions of Si and Ge by the C adatom or briefly S-type bindings are energetically favorable since Si−C and Ge−C bonds are stronger than Si−Si and Ge−Ge bonds, respectively. Additionally, the C adatom substituting Si or Ge host atoms becomes 3-fold coordinated. Substitution energies are rather high and calculated as 5.89 and 5.02 eV for silicene and germanene, respectively. This situation suggests that one can generate new derivatives from silicene and germanene through C substitution. On the other hand, the interactions of Si, Ge, and Sn with the graphene substrate and resulting binding structures are different. Since the length of a C−C bond in graphene is smaller than Si−C, Ge−C, and Sn−

dx.doi.org/10.1021/jp5106554 | J. Phys. Chem. C 2015, 119, 845−853

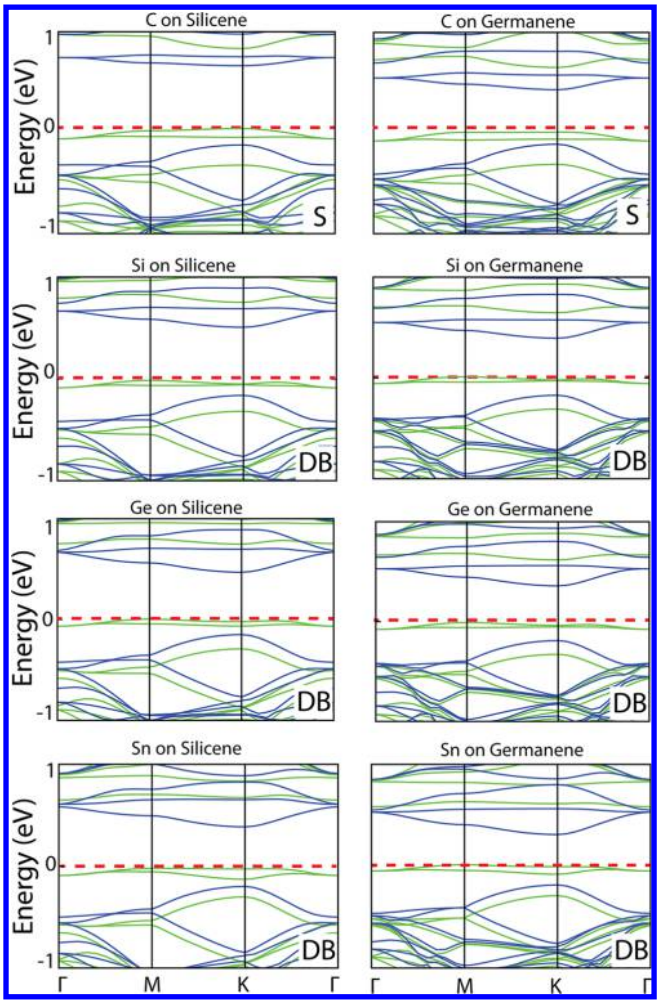

Figure 5. Electronic band structures are calculated by using HSE for single-layer silicene and germanene with adatoms C, Si, Ge, and Sn, which form a 5 × 5 supercell or pattern. In the spin-polarized systems, spin up and spin down bands are shown with green and blue lines. The zero of energy shown by a red dashed line is set to the energy of the highest occupied state. Binding structures (as B, S, DB) are indicated in each panel.

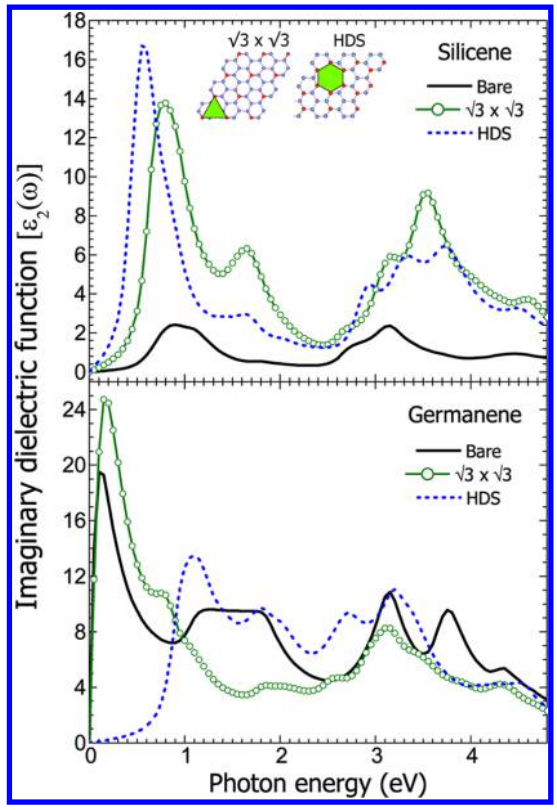

Figure 6. Optical absorption spectra of bare (black curve), ($\sqrt{3} \times \sqrt{3}$) (green curve with dots), and HDS (dashed blue curve) structures of silicene (top) and germanene (bottom), respectively. Structures are shown in the inset plots.

C bonds, Si, Ge, and Sn adatoms adsorbed on graphene favor bridge bonds shown in Figure 1(a), where the top and hollow sites are 0.09 and 0.57 eV less favorable, respectively.[42]

Energetically the most favorable binding structure of Si, Ge, and Sn adatoms on silicene and germanene is the DB structure as described in the lower panel of Figure 1. The adatom (D_1) is first adsorbed on top of the host silicene or germanene. Subsequently it pushes down the host atom underneath (D_2) to form a DB consisting of D_1 and D_2 atoms. While D_1 lies above the substrate plane, D_2 is below, and each one is bonded to three host atoms. The distance between D_1 and D_2 is relatively larger than the first nearest-neighbor distance, and consequently the bonding between them is weak. In this study, the DB atoms (D_1 and D_2) can be various combinations of Group IV elements of the periodic table. However, owing to its weak stability, adsorption of Si, Ge, and Sn adatoms on stanene does not form DB structures; rather, they undergo local structural instability, followed by local destruction of single-layer honeycomb structure upon adsorption of Si, Ge, and Sn adatoms. Instability occurred not only in the course structure optimization of the adatom + stanene system using structure optimization using the conjugate gradient method but also in the *ab initio* MD calculations at low temperature.

DB structures form without any energy barrier once Si, Ge, and Sn adatoms are placed on silicene or germanene.[23] The DB structure is of particular interest since specific periodic patterns of DBs on silicene or germanene can construct stable derivative structures which can have higher cohesive energy with different electronic and magnetic properties compared to parent silicene and germanene.[8,21,24,27] These derivatives were shown to be crucial for the growth of multilayer silicene and germanene on Ag and Au substrates, respectively.[27] In fact, stacking of these derivatives can make stable thin films[7,27] or 3D bulk layered structures, namely, silicite and germanite, displaying rather different electronic and optical properties.[21] Briefly, the synthesis of derivatives composed of silicene and germanene patterned by DBs of Si or Ge and their alloys paves the way toward nanostructures with physical properties different from their parent cubic diamond structure, cdSi or cdGe. Our results obtained from structure optimization indicate that the binding energy of a single DB on silicene and germanene is rather high and ranges between 4.01 and 3.08 eV. Generally, while the binding energies decrease, D_1-D_2 distances increase as the row number of the Group IV adatom increases. We note that DB patterned phases of silicene and germanene display a side view of atoms; in particular, D_1 and D_2 nematic orbitals are reminiscent of X−X bonds of transition metal dichalcogenides, MX_2.[26] However, the FDS structure consisting of silicene having three DBs at the alternating corners of hexagon, which is, in fact, very similar to single-layer MX_2, was found to be unstable.[27]

dx.doi.org/10.1021/jp5106554 | J. Phys. Chem. C 2015, 119, 845−853

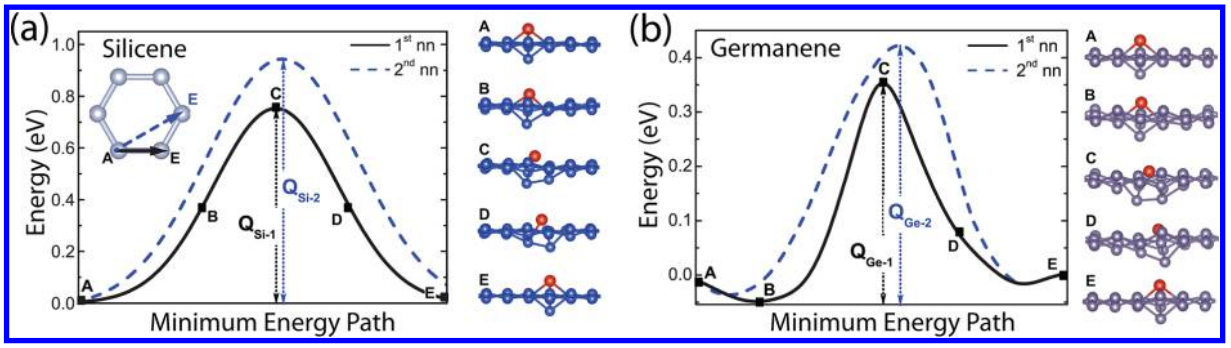

Figure 7. (a) Migration of Si-DB on silicene and (b) Ge-DB on germanene. Energetics and the migration energy barrier (Q) of a single, isolated DB between the first and second nearest neighbors are shown by the inset in the left panel. The barriers are calculated using the nudged elastic band (NEB) method. Snapshots of the atomic configurations taken at stages A, B, C, D, and E during the migration of DB to the first nearest-neighbor site are also presented to illustrate the mechanism of diffusion.

It is known that single-layer Group IV−IV compounds, like SiC and SiGe,[6] can be constructed. In SiC, Si and C atoms are located at the alternating corners of the hexagon to make a planar, graphene-like structure with a 2.5 eV indirect band gap. Here, the binding structures of C and Si adatoms on C and Si host atoms of SiC are of interest. In spite of the fact that the C adatom is adsorbed at the B-site on graphene and substitutes the Si host atom on silicene, the C adatom forms a DB structure on SiC when placed on top of the host C atom. While the DB structure made of two C atoms is the second most energetic binding structure of graphene,[42] DB of C atoms becomes the most energetic binding structure in SiC. On the other hand, the C adatom on top of host Si, the Si adatom on top of host C, and the Si adatom on top of the host Si atom of SiC are bound at the top site (T). Even if the adatoms were displaced from the top site or were placed to the B-site, they always moved to the equilibrium T site to minimize the total energy. In Figure 2, these four equilibrium binding structures, each with a magnetic moment of 2.0 μ_B/per cell, are illustrated.

The SiGe honeycomb structure, where Si and Ge atoms are alternatingly located at the corner of the hexagon, is another important compound we considered in this study. The buckling between adjacent Si and Ge is larger than that in silicene but smaller than that in germanene. It is stable and has $\pi-\pi^*$ bands crossing linearly at the Fermi level, if small spin−orbit coupling is neglected. Four types of DBs, namely, Si−Si, Ge−Si, Si−Ge, and Ge−Ge DBs, can be constructed, each having a magnetic ground state of 2.0 μ_b/per cell, but attributing different physical properties to the SiGe substrate.

The crucial issue to address now is whether the adatom adsorbed substrates are stable. While the optimized structure through the conjugate gradient method provides evidence that the structure in hand is stable at T = 0 K, this may correspond to a shallow minimum, and hence the system may be destabilized at elevated temperatures. In fact, we found that the adsorption of all Group IV adatoms caused stanene to undergo a structural instability. Here we explored the stability of Group IV adatoms adsorbed on silicene and germanene at elevated temperature by performing *ab initio* MD calculations at finite temperatures, whose details are explained in the Methods section. Even at a temperature as high as T = 1500 K, the systems presented in Table 1 remained stable. We also note that similar MD calculations were carried out to test whether bare stanene by itself is stable at elevated temperatures. While free-standing stanene maintained its structural stability for one picosecond at 400 K, its structure is massively deformed during MD simulation at 600 K. This explains why the structure of stanene is destroyed upon the adsorption of Group IV atoms treated in this study. It should be noted that stanene grown on a substrate can attain stability and remain stable upon the adsorption of adatoms.

Electronic Structures. Group IV adatoms give rise to important changes also in the magnetic and electronic properties. In Figure 3 we presented the total density of states for C, Si, and Ge adatoms adsorbed on graphene, silicene, and germanene, respectively. The partial density of states of adatoms depicts the contribution of the adatom in the relevant energy range. For the sake of comparison, the density of states of the corresponding bare substrate is also shown in each panel. While bare graphene, silicene, and germanene all have a nonmagnetic ground state, they attain a magnetic ground state upon the adsorption of adatoms. The dominant effect of the adatom appears as sharp peaks near the band edges, which originate from the flat bands constructed from the mixing of orbitals of adatoms and host atoms at close proximity. In Figure 4 we present the electronic band structures of the optimized structures for C, Si, Ge, and Sn adatoms adsorbed also on graphene, silicene, and germanene. In addition, we improve the band structures with HSE as shown in Figure 5. Similar to binding structure and energetics of the adatom, the effects of the adatom on the electronic and magnetic structures are explored using a supercell model. If the spin−orbit coupling is neglected, bare graphene, silicene, as well as germanene are semimetals with conduction and valence bands crossing linearly at the Fermi level (E_F) carrying massless Dirac Fermion behavior.[2] The localized (or resonance) states of single, isolated Group IV adatoms can occur below or above their E_F. However, within the periodically repeating 5 × 5 supercell model with minute DB−DB coupling, these states are slightly broadened and form adatom bands. Therefore, the flat bands in Figure 4 are associated with the localized states due to adatoms. The effect of the adatoms on the electronic and magnetic properties are summarized also in Table 1. On silicene and germanene they lead to similar electronic and magnetic states. DB formations on silicene and germanene in 5 × 5 supercell periodicity result in ferromagnetic semiconductors with small band gaps of 0.06−0.12 eV within the DFT-GGA. The magnetic moment per supercell is calculated to be 2.0 μ_B. The energy difference between the magnetic and nonmagnetic state is rather small (∼0.1 eV) for all cases indicating that it is a low-temperature property. In what follows we present a comprehensive analysis of electronic band structures.

dx.doi.org/10.1021/jp5106554 | J. Phys. Chem. C 2015, 119, 845−853

In Figure 4, flat bands at the E_F are associated with the states localized at the carbon adatom at the B-site forming bridge bonds with two nearest-neighbor C atoms of graphene. These bands, which pin the E_F are derived from p_y and p_z orbitals of the carbon adatom at the B-site. In the 5 × 5 supercell, the crossing bands of bare graphene split, and E_F dips into the valence band to attribute metallic character. The net magnetic moment of each supercell is $\mu = 1.6\ \mu_B$. Si, Ge, and Sn adatoms, which are also bonded to graphene at the B-site, give rise to metallic band structures as shown in Figure 4. The $\pi^*-\pi$ bands of bare graphene, which cross linearly at the K-point of the Brillouin zone, dip 0.1−0.3 eV below the E_F upon the adsorption of Si, Ge, and Sn adatoms at the B-site. It appears that the flat bands associated with the localized p-orbital states of Si, Ge, and Sn adsorbates occur above the band crossing point and pin the E_F. In addition, each supercell attains a magnetic moment of 2 μ_B. This is a significant effect, which makes nonmagnetic graphene, silicene, and germanene spin-polarized.

The flat bands shown in Figure 4 near the band gap of the substitutional C adatom forming a 5 × 5 pattern in silicene and germanene are associated with the localized (or resonance) p-orbital states of the adatom as well as the p-orbital states of the host Si atom that is displaced from its regular position as indicated by the small arrow in Figure 1(b). The effect of the substitutional C atom is the splitting of the $\pi^*-\pi$ bands crossing at the k-point and hence transforming the semimetal bare silicene/germanene to a semiconductor. The lower valence bands are also affected by the substitutional C atom.

Upon the formation of Si-DB on silicene the spin degeneracy of the bands is lifted as shown in Figure 4, and a narrow band gap opens between spin up and spin down bands. It should be noted that the electronic and magnetic properties of silicene patterned by Si-DB strongly depend on the size and symmetry of the DB pattern. Similar effects occur also with Ge-DB and Sn-DB forming a 5 × 5 pattern in silicene and germanene, except that the band gap between spin up and spin down bands is closed as the row number of adatom increases.

Considering the fact that the energy band gaps are underestimated by standard DFT methods, we repeat the calculations by using hybrid functionals,[34] except for graphene where all configurations are metallic. According to those results all the systems are ferromagnetic semiconductor confirming what is obtained at the DFT-GGA level with an expected increase in energy band gaps. The corrected band gaps are given in parentheses in Table 1. Interestingly, energy band gaps decrease as the row number of the adatom as well as the substrate increase.

The optical properties of the two 2D honeycomb Group IV crystals; silicene and germanene have been briefly investigated by calculating the frequency-dependent complex dielectric function $\varepsilon_i(\omega)$ for normal incidence. The optical absorption is determined by the imaginary part of the dielectric function. The main peaks of absorption of both structures are related with the interband transitions that come into play. This finding is also supported in the works which study the infrared absorption spectra of silicene and germanene.[43,44] In fact, both materials are known to be attractive candidates for nano-optoelectronic applications since they display electronic and optical bandgaps which are within or in the vicinity of the visible part of the electromagnetic spectrum. Here the effects of Si and Ge adatoms are investigated by comparing the calculated optical properties before and after dumbbell formation. Two different coverages of dumbbells leading to $(\sqrt{3} \times \sqrt{3})$ dumbbell structure and hexagonal dumbbell structure (HDS) were investigated.[8,27] The imaginary dielectric function is displayed in Figure 6 for both systems. Accordingly, bare silicene shows optical activity around 1 eV in the relatively early frequency regime, which extends to beyond 3 eV toward higher photon energies. As for the $(\sqrt{3} \times \sqrt{3})$ and HDS supercells of silicene, intense peaks of absorption are observed around 0.6 and 0.8 eV, respectively. Moreover, the second major peaks for both are concentrated in the range of 2.8−4.4 eV. $\varepsilon_2(\omega)$ of bare germanene, on the other hand, displays more similar features to its doped counterparts, when compared to silicene. An early strong absorption phenomenon takes place below 0.3 eV for both bare and $(\sqrt{3} \times \sqrt{3})$ forms of germanene. On the contrary, Ge-HDS shows a first peak around 1.1 eV. Some important preliminary results can be summarized as: (i) The intensities of the absorption peaks vary (i.e., become more distinguished) depending on the structure, when doped. (ii) The optically active region can be tuned by doping. Apparently, the periodic structure of DBs may introduce crucial effects on the optical absorption spectra, which may lead to certain potential applications in the visible range. Further investigation of the optical properties of DB structures of silicene and germanene is considered as the topic of a future publication, which are aimed to be studied also at the level of many-body perturbation theory in order to introduce further accuracy to the peaks of absorption.

Migration of Dumbbells on Silicene and Germanene. As mentioned above, as soon as specific adatoms land on specific substrates, DBs can form through an exothermic process without an energy barrier. Moreover, DB−DB coupling is attractive until the first nearest-neighbor separation.[8,24] Consequently, as Si, Ge, and Sn adatoms continue to land on silicene or germanene, first the domains of DBs form, and eventually they join to cover the surface uniformly. In this respect, the migration or diffusion of DBs on silicene and germanene is crucial for the formation of various phases derived from silicene and germanene through their coverage by DBs in different concentration and symmetry. The energetics of the migration and the minimum energy barrier of single Si-DB on silicene and Ge-DB on germanene are investigated between the first and second nearest neighbors as shown in Figure 7 using the nudged elastic band (NEB) method.[45] The difference of the maximum and minimum total energy along the path corresponds to the energy barrier, Q. The energy barrier to the migration of D_1 of Si-DB along the straight path between the two first nearest-neighbor atoms of silicene is $Q = 0.75$ eV (minima are denoted by A and maxima by C in Figure 7). Similar to the binding energies in Table 1, the diffusion barrier of Ge-DB on germanene is lower than that of Si-DB on silicene. The barrier along the path between the second nearest neighbor is slightly higher. In a concerted action, as D_1 moves along the path, D_2 raises and eventually attains its original position at the corner of the buckled hexagon. On the contrary, the host atom at the first nearest-neighbor site moves down as D_1 approaches, and eventually the migration is completed with the construction of a new DB at the first nearest-neighbor site. Snapshots of atomic structure in the course of migration is also in shown Figure 7. The low-energy barrier to migration assures high mobility of DBs on silicene and germanene substrates needed for multilayer growth. The local minimum denoted by B (which is energetically lower than A) for Ge-DB on germanene is considered to be due to a local

dx.doi.org/10.1021/jp5106554 | J. Phys. Chem. C 2015, 119, 845−853

unstable deformation appearing at that instantaneous atomic arrangement.

CONCLUSIONS

In this paper we investigated the binding of Group IV adatoms (C, Si, Ge, and Sn) to single-layer, honeycomb structures of these atoms, namely, graphene, silicene, and germanene. The adsorption to stanene is not included since this structure is prone to instability upon the adsorption of any of the Group IV adatoms. Depending on the row number of a Group IV adatom, as well as substrates, we deduced three types of equilibrium binding structures. Isolated adatoms, as well as those forming periodically repeating supercells on graphene, silicene, and germanene, give rise to changes in electronic, magnetic, and optical properties. Among the three types of binding structures, the dumbbell structure is of particular importance since stable new phases of silicene and germanene can be derived from their periodic coverage with DBs. Dumbbell structures are also constructed on single-layer, Group IV–IV compounds. The calculated energy barrier to the migration or diffusion of DBs on substrates is found to be low. This implies that DBs are rather mobile and cover the substrates as long as there is a sufficient amount of incoming adatoms. By stacking these single-layer phases one can grow thin-film alloys and layered bulk structure of silicene and germanene.

AUTHOR INFORMATION

Corresponding Authors

*E-mail: durgun@unam.bilkent.edu.tr

*E-mail: ciraci@fen.bilkent.edu.tr.

Notes

The authors declare no competing financial interest.

ACKNOWLEDGMENTS

The computational resources are provided by TUBITAK ULAKBIM, High Performance and Grid Computing Center (TR-Grid e-Infrastructure). VOÖ and SC acknowledge financial support from the Academy of Sciences of Turkey (TUBA). ED acknowledges support from Bilim Akademisi - The Science Academy, Turkey under the BAGEP program. This work is partially supported by TUBITAK under the Project No. 113T050.

REFERENCES

(1) Durgun, E.; Tongay, S.; Ciraci, S. Silicon and III-V Compound Nanotubes: Structural and Electronic Properties. *Phys. Rev. B* **2005**, *72*, 075420.

(2) Cahangirov, S.; Topsakal, M.; Aktürk, E.; Şahin, H.; Ciraci, S. Two- and One-Dimensional Honeycomb Structures of Silicon and Germanium. *Phys. Rev. Lett.* **2009**, *102*, 236804.

(3) De Padova, P.; Quaresima, C.; Ottaviani, C.; Sheverdyaeva, P. M.; Moras, P.; Carbone, C.; Topwal, D.; Olivieri, B.; Kara, A.; Oughaddou, H.; Aufray, B.; Le Lay, G. Evidence of Graphene-like Electronic Signature in Silicene Nanoribbons. *Appl. Phys. Lett.* **2010**, *96*, 261905.

(4) Vogt, P.; De Padova, P.; Quaresima, C.; Avila, J.; Frantzeskakis, E.; Asensio, M. C.; Resta, A.; Ealet, B.; Le Lay, G. Silicene: Compelling Experimental Evidence for Graphenelike Two-Dimensional Silicon. *Phys. Rev. Lett.* **2012**, *108*, 155501.

(5) Van Hoang, V.; Mi, H. T. C. Free-standing Silicene Obtained by Cooling from 2D Liquid Si: Structure and Thermodynamic Properties. *J. Phys. D: Appl. Phys.* **2014**, *47*, 495303.

(6) Şahin, H.; Cahangirov, S.; Topsakal, M.; Bekaroglu, E.; Akturk, E.; Senger, R. T.; Ciraci, S. Monolayer Honeycomb Structures of Group-IV Elements and III-V Binary Compounds: First-Principles Calculations. *Phys. Rev. B* **2009**, *80*, 155453.

(7) De Padova, P.; Vogt, P.; Resta, A.; Avila, J.; Razado-Colambo, I.; Quaresima, C.; Ottaviani, C.; Olivieri, B.; Bruhn, T.; Hirahara, T.; Shirai, T.; Hasegawa, S.; Carmen Asensio, M.; Le Lay, G. Evidence of Dirac Fermions in Multilayer Silicene. *Appl. Phys. Lett.* **2013**, *102*, 163106.

(8) Özçelik, V. O.; Durgun, E.; Ciraci, S. New Phases of Germanene. *J. Phys. Chem. Lett.* **2014**, *5*, 2694–2699.

(9) Rachel, S.; Ezawa, M. Giant Magnetoresistance and Perfect Spin Filter in Silicene, Germanene, and Stanene. *Phys. Rev. B* **2014**, *89*, 195303.

(10) Özçelik, V. O.; Cahangirov, S.; Ciraci, S. Stable Single-Layer Honeycomblike Structure of Silica. *Phys. Rev. Lett.* **2014**, *112*, 246803.

(11) Xu, Y.; Yan, B.; Zhang, H.-J.; Wang, J.; Xu, G.; Tang, P.; Duan, W.; Zhang, S.-C. Large-Gap Quantum Spin Hall Insulators in Tin Films. *Phys. Rev. Lett.* **2013**, *111*, 136804.

(12) Liu, C.-C.; Jiang, H.; Yao, Y. Low-energy Effective Hamiltonian Involving Spin-orbit Coupling in Silicene and Two-dimensional Germanium and Tin. *Phys. Rev. B* **2011**, *84*, 195430.

(13) Tang, P.; Chen, P.; Cao, W.; Huang, H.; Cahangirov, S.; Xian, L.; Xu, Y.; Zhang, S.-C.; Duan, W.; Rubio, A. Stable Two-dimensional Dumbbell Stanene: A Quantum Spin Hall Insulator. *Phys. Rev. B* **2014**, *90*, 121408.

(14) Van den Broek, B.; Houssa, M.; Scalise, E.; Pourtois, G.; Afanasev, V. V.; Stesmans, A. Two-dimensional Hexagonal Tin: Ab Initio Geometry, Stability, Electronic Structure and Functionalization. *2D Mater.* **2014**, *1*, 021004.

(15) Ataca, C.; Sahin, H.; Ciraci, S. Stable, Single-layer MX_2 Transition Metal Oxides and Dichalcogenides in a Honeycomb-like Structure. *J. Phys. Chem. C* **2012**, *116*, 8983–8999.

(16) Tongay, S.; Zhou, J.; Ataca, C.; Lo, K.; Matthews, T. S.; Li, J.; Grossman, J. C.; Wu, J. Thermally Driven Crossover from Indirect toward Direct Bandgap in 2D Semiconductors: $MoSe_2$ versus MoS_2. *Nano Lett.* **2012**, *12*, 5576–5580.

(17) Novoselov, K. S.; Jiang, D.; Schedin, F.; Booth, T. J.; Khotkevich, V. V.; Morozov, S. V.; Geim, A. K. Two-dimensional Atomic Crystals. *Proc. Natl. Acad. Sci. U.S.A.* **2005**, *102*, 10451–10453.

(18) Wang, Z.; Zhao, K.; Li, H.; Liu, Z.; Shi, Z.; Lu, J.; Suenaga, K.; Joung, S.-K.; Okazaki, T.; Jin, Z.; Gu, Z.; Gao, Z.; Iijama, S. Ultra-narrow WS_2 Nanoribbons Encapsulated in Carbon Nanotubes. *J. Mater. Chem.* **2011**, *21*, 171–180.

(19) Vogt, P.; Capiod, P.; Berthe, M.; Resta, A.; De Padova, P.; Bruhn, T.; Le Lay, G.; Grandidier, B. Synthesis and Electrical Conductivity of Multilayer Silicene. *Appl. Phys. Lett.* **2014**, *104*, 021602.

(20) Padova, P. D.; Ottaviani, C.; Quaresima, C.; Olivieri, B.; Imperatori, P.; Salomon, E.; Angot, T.; Quagliano, L.; Romano, C.; Vona, A.; Muniz-Miranda, M.; Generosi, A.; Paci, B.; Lay, G. L. 24h Stability of Thick Multilayer Silicene in Air. *2D Mater.* **2014**, *1*, 021003.

(21) Cahangirov, S.; Özçelik, V. O.; Rubio, A.; Ciraci, S. Silicite: The Layered Allotrope of Silicon. *Phys. Rev. B* **2014**, *90*, 085426.

(22) Tritsaris, G. A.; Kaxiras, E.; Meng, S.; Wang, E. Adsorption and Diffusion of Lithium on Layered Silicon for Li-ion Storage. *Nano Lett.* **2013**, *13*, 2258–2263.

(23) Özçelik, V. O.; Gurel, H. H.; Ciraci, S. Self-healing of Vacancy Defects in Single-layer Graphene and Silicene. *Phys. Rev. B* **2013**, *88*, 045440.

(24) Özçelik, V. O.; Ciraci, S. Local Reconstructions of Silicene Induced by Adatoms. *J. Phys. Chem. C* **2013**, *117*, 26305–26315.

(25) Kaltsas, D.; Tsetseris, L. Stability and Electronic Properties of Ultrathin Films of Silicon and Germanium. *Phys. Chem. Chem. Phys.* **2013**, *15*, 9710–9715.

(26) Gimbert, F.; Lee, C.-C.; Friedlein, R.; Fleurence, A.; Yamada-Takamura, Y.; Ozaki, T. Diverse Forms of Bonding in Two-dimensional Si Allotropes: Nematic Orbitals in the MoS_2 Structure. *Phys. Rev. B* **2014**, *90*, 165423.

(27) Cahangirov, S.; Özçelik, V. O.; Xian, L.; Avila, J.; Cho, S.; Asensio, M. C.; Ciraci, S.; Rubio, A. Atomic Structure of the $\sqrt{3}\times\sqrt{3}$ Phase of Silicene on Ag(111). *Phys. Rev. B* **2014**, *90*, 035448.
(28) Kohn, W.; Sham, L. J. Self-Consistent Equations Including Exchange and Correlation Effects. *Phys. Rev.* **1965**, *140*, A1133−A1138.
(29) Hohenberg, P.; Kohn, W. Inhomogeneous Electron Gas. *Phys. Rev.* **1964**, *136*, B864−B871.
(30) Grimme, S. Semiempirical GGA-type Density Functional Constructed with a Long-Range Dispersion Correction. *J. Comput. Chem.* **2006**, *27*, 1787−1799.
(31) Blöchl, P. E. Projector Augmented-wave Method. *Phys. Rev. B* **1994**, *50*, 17953−17979.
(32) Perdew, J. P.; Burke, K.; Ernzerhof, M. Generalized Gradient Approximation Made Simple. *Phys. Rev. Lett.* **1996**, *77*, 3865−3868.
(33) Kresse, G.; Furthmüller, J. Efficient Iterative Schemes for Ab-initio Total-energy Calculations Using a Plane-wave Basis set. *Phys. Rev. B* **1996**, *54*, 11169−11186.
(34) Paier, J.; Marsman, M.; Hummer, K.; Kresse, G.; Gerber, I. C.; Ángyán, J. G. Screened Hybrid Density Functionals Applied to Solids. *J. Chem. Phys.* **2006**, *124*, 154709.
(35) Heyd, J.; Scuseria, G. E.; Ernzerhof, M. Hybrid functionals based on a screened Coulomb potential. *J. Chem. Phys.* **2003**, *118*, 8207−8215.
(36) Gajdoš, M.; Hummer, K.; Kresse, G.; Furthmüller, J.; Bechstedt, F. Linear Optical Properties in the Projector-augmented Wave Methodology. *Phys. Rev. B* **2006**, *73*, 045112.
(37) Tongay, S.; Senger, R. T.; Dag, S.; Ciraci, S. Ab-initio Electron Transport Calculations of Carbon Based String Structures. *Phys. Rev. Lett.* **2004**, *93*, 136404.
(38) Fan, X. F.; Liu, L.; Lin, J. Y.; Shen, Z. X.; Kuo, J.-L. Density Functional Theory Study of Finite Carbon Chains. *ACS Nano* **2009**, *3*, 3788−3794.
(39) Özçelik, V. O.; Ciraci, S. Self-assembly Mechanisms of Short Atomic Chains on Single-layer Graphene and Boron Nitride. *Phys. Rev. B* **2012**, *86*, 155421.
(40) Ataca, C.; Ciraci, S. Perpendicular Growth of Carbon Chains on Graphene from First-principles. *Phys. Rev. B* **2011**, *83*, 235417.
(41) Ataca, C.; Aktürk, E.; Şahin, H.; Ciraci, S. Adsorption of Carbon Adatoms to Graphene and Its Nanoribbons. *J. Appl. Phys.* **2011**, *109*, 013704.
(42) Aktürk, E.; Ataca, C.; Ciraci, S. Effects of Silicon and Germanium Adsorbed on Graphene. *Appl. Phys. Lett.* **2010**, *96*, 123112.
(43) Matthes, L.; Gori, P.; Pulci, O.; Bechstedt, F. Universal Infrared Absorbance of Two-Dimensional Honeycomb Group-IV Crystals. *Phys. Rev. B* **2013**, *87*, 035438.
(44) Matthes, L.; Pulci, O.; Bechstedt, F. Massive Dirac Quasiparticles in the Optical Absorbance of Graphene, Silicene, Germanene, and Tinene. *J. Phys.: Condens. Matter* **2013**, *25*, 395305.
(45) Henkelman, G.; Uberuaga, B. P.; Jónsson, H. A Climbing Image Nudged Elastic Band Method for Finding Saddle Points and Minimum Energy Paths. *J. Chem. Phys.* **2000**, *113*, 9901−9904.